Ultrafast spin and lattice dynamics in antiferromagnetic Cr_2O_3

Takuya Satoh,* Bas B. Van Aken,† Nguyen Phuc Duong,‡ Thomas Lottermoser,§ and Manfred Fiebig‖
Max-Born-Institut, Max-Born-Straße 2A, 12489 Berlin, Germany

(Received 7 November 2006; revised manuscript received 5 February 2007; published 9 April 2007)

The spin and lattice dynamics of antiferromagnetic bulk Cr_2O_3 after excitation with an intense laser pulse were investigated using amplitude and phase resolved optical second-harmonic generation as probe of the magnetic and crystallographic subsystems. Demagnetization occurs on three time scales ranging from $\ll 1$ to ~ 7 ps. In comparison to ferromagnetic compounds, this is a two orders of magnitude faster response and an additional spin-lattice interaction channel is observed.

DOI: 10.1103/PhysRevB.75.155406 PACS number(s): 78.47.+p, 42.65.Ky, 75.50.Ee, 78.20.Ls

I. INTRODUCTION: SPIN DYNAMICS OF ANTIFERROMAGNETIC COMPOUNDS

One of the aspects steering the development of data-storage technologies is the speed at which the magnetic state can be manipulated. Therefore, dynamical processes in magnetically ordered systems are a key issue of the rapidly evolving field of spin electronics. For ferromagnetic systems, it was shown that magnetic-field pulses allow repeated switching of the magnetization on the subnanosecond time scale, while optical experiments with pulsed lasers revealed demagnetization processes down to the subpicosecond range.[1–3] In spite of the increasing interest in antiferromagnetic (AFM) systems for practical applications,[4,5] their magnetization dynamics is less well understood. This is mostly due to the absence of a macroscopic magnetization which impedes direct access to the AFM order parameter. Therefore, secondary effects are employed to study the spin dynamics of AFM systems on the ultrafast time scale: a weak ferromagnetic moment accompanying the AFM order (as in $FeBO_3$),[6] a change of birefringence induced by AFM reordering (as in orthoferrites),[7] a change of reflectivity characteristic for the melting of an AFM insulating state (as in $Pr_{0.7}Ca_{0.3}MnO_3$),[8] or the exchange-bias effect (as in NiO/NiFe bilayers).[9] However, the more indirect the coupling to the AFM order parameter is, the more difficult it gets to disentangle magnetic and crystallographic contributions to the response signal and, thus, to distinguish between the dynamics of the spins and the lattice. The problem may be solved by resorting to *nonlinear* instead of *linear* optical techniques. Second-harmonic generation (SHG) possesses contributions that couple either to the "spinless" crystal or to the magnetic order parameter. Therefore, it distinguishes very efficiently between the crystallographic and magnetic properties of, in particular, AFM compounds or ferromagnetic surfaces and interfaces.[10–13]

In this paper, we describe the temporal evolution of spins and lattice in AFM Cr_2O_3 bulk crystals after excitation with an intense 250 fs laser pulse. The dynamical response of the two subsystems is probed in one experimental run by SHG coupling to the AFM order parameter or to the crystal structure. The *amplitude* of the SHG signals reveals a different response of spins and lattice. The *phase* between the SHG contributions leads to the identification of three demagnetization channels on separate time scales. Distinct differences to the dynamics of ferromagnetic systems are observed.

II. MAGNETIC AND CRYSTALLOGRAPHIC SECOND-HARMONIC GENERATION

The simplest nonlinear optical process is SHG with

$$S_i(2\omega) = \varepsilon_0 \chi_{ijk} E_j(\omega) E_k(\omega), \tag{1}$$

where $\vec{E}(\omega)$ is the electric field of the incident light wave at frequency ω, while $\vec{S}(2\omega)$ is the source of the light wave at the frequency 2ω emitted from the crystal.[14] The light-matter interaction is parametrized by the susceptibility $\hat{\chi}$. The tensor $\hat{\chi}=\hat{\chi}(0)+\hat{\chi}(\ell)+\ldots$ is expanded in the magnetic order parameter ℓ. $\hat{\chi}(0)$ represents the "crystallographic" contributions found above and below the magnetic ordering temperature, while $\hat{\chi}(\ell)$ is the leading "magnetic" contribution found below the ordering temperature only.[15] SHG from $\hat{\chi}(\ell)$ and $\hat{\chi}(0)$ can thus be used to probe the spins and the lattice, respectively, and, thus, to reveal their coupling.

III. Cr_2O_3 AS MODEL COMPOUND

Our interest in Cr_2O_3 is twofold: On the one hand, recent interest in this compound was triggered by its exchange-bias properties,[16] which can be controlled via the magnetoelectric effect.[17] The magnetoelectric interaction depends on the correlation between spins and lattice. This warrants an investigation of this correlation. On the other hand, Cr_2O_3 is an AFM model compound whose static properties are well known.[18] This is an ideal basis for investigating its dynamical properties. Note that the spin-wave dynamics of Cr_2O_3 has already been studied,[19] however, without observing the dynamics of the spin-lattice energy transfer.

Cr_2O_3 is a uniaxial antiferromagnet crystallizing in the centrosymmetric point group $\bar{3}m$.[18] The structure is composed of chains of Cr^{3+} ions aligned along the trigonal z axis. The Cr^{3+} ions are surrounded by distorted octahedra of O^{2-} ions with 3 as site symmetry. Cr_2O_3 orders antiferromagnetically at $T_N=307.6$ K.[18] The sequence of Cr^{3+} spins along z in the unit cell of opposite 180° domains is $+-\cdot+-$ and $-+\cdot-+$, where the dot denotes an empty, undistorted O^{2-} octahedron. The AFM order breaks both time and space inversion symmetry and leads to $\bar{3}m$ as magnetic point symmetry.[20] The contributions from $\hat{\chi}(0)$ and $\hat{\chi}(\ell)$ to the source term $\vec{S}$ of the SHG wave described by Eq. (1) were derived in Ref. 20 and are summarized as follows: With light incident along the trigonal z axis, only one independent com-

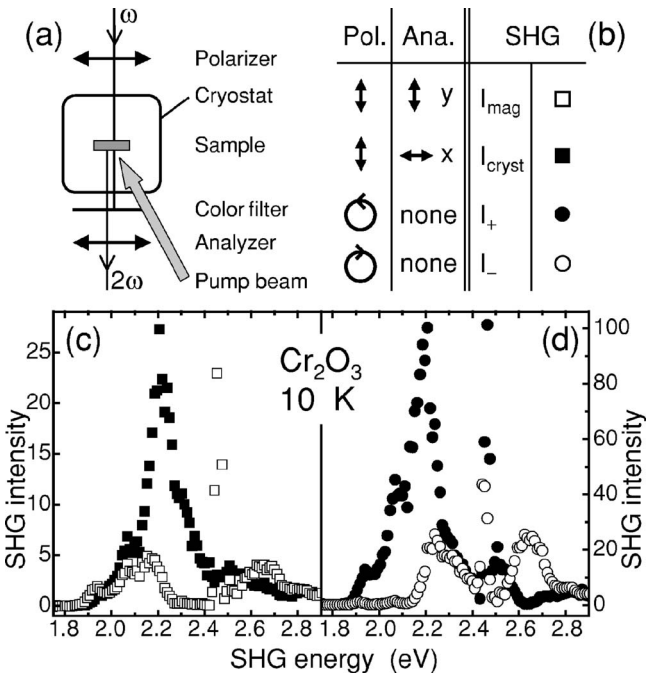

FIG. 1. Experimental setup and SHG spectra of Cr_2O_3 measured in one experimental run at 10 K for light incident along the z axis. (a) Setup for pump-and-probe experiments with SHG in transmission as probe process. (b) Settings of polarizer (a quarter-wave plate) and analyzer (a polarization foil) needed to obtain the amplitude of and the phase between spin and lattice contributions to the SHG signal. The y and x axes of Cr_2O_3 are defined by lying, respectively, perpendicular to and in the mirror plane of the crystal with $\bar{3}m$ symmetry (Ref. 18). (c) Spectra of the magnetic and crystallographic contributions to SHG. (d) Spectra of their constructive and destructive interferences.

ponent from the tensors $\hat{\chi}(0)$ and $\hat{\chi}(\ell)$ contributes to SHG, which is henceforth simply denoted as $\chi(0)$ and $\chi(\ell)$, respectively. One gets

$$\vec{S} = \begin{pmatrix} S_x \\ S_y \\ S_z \end{pmatrix} = 4\frac{\omega^2}{c^2} \begin{pmatrix} \chi(0)(E_x^2 - E_y^2) + 2\chi(\ell)E_xE_y \\ -2\chi(0)E_xE_y + \chi(\ell)(E_x^2 - E_y^2) \\ 0 \end{pmatrix}, \quad (2)$$

for linearly polarized light, and

$$\vec{S} = \begin{pmatrix} S_+ \\ S_- \\ S_0 \end{pmatrix} = 4\sqrt{2}\frac{\omega^2}{c^2} \begin{pmatrix} [-\chi(0) + i\chi(\ell)]E_-^2 \\ [+\chi(0) + i\chi(\ell)]E_+^2 \\ 0 \end{pmatrix}, \quad (3)$$

for circularly polarized light. According to Eq. (2), a polarization analysis allows one to separate spin and lattice contributions to SHG: With light incident along the z axis and polarized linear along one of the principal axes, the x- and the y-polarized components of the corresponding SHG wave couple to $\chi(0)$ and $\chi(\ell)$, respectively. On the other hand, use of circularly polarized light allows one to obtain the constructive and destructive interferences of SHG contributions from $\chi(0)$ and $\chi(\ell)$.

IV. EXPERIMENTAL SETUP

Cr_2O_3 crystals grown by the flux method were oriented by Laue diffraction and cut perpendicular to the trigonal z axis by a diamond saw. Lapping by SiC powder was followed by chemical mechanical polishing with a colloidal silica slurry (Syton). The finalized samples had a lateral size of a few millimeters and a thickness of ~ 50 μm. They were mounted in a cryostat, and areas located within one AFM domain were studied in two types of transmission experiments: (i) SHG spectra were measured using 5 ns laser pulses at a repetition rate of 10 Hz, which were emitted from an optical parametric oscillator pumped by the third harmonic of a Nd-doped yttrium aluminum garnet laser. (ii) The temporal evolution of the SHG signal was measured in a pump-and-probe experiment. The samples were excited at $\hbar\omega_{pump}=3.10$ eV with 250 fs pulses at an intensity of 1–10 mJ/cm^2. The pulses were generated at a repetition rate of 1 kHz by frequency doubling amplified pulses at 1.55 eV emitted from a Ti:sapphire laser. Because of the proximity to the charge-transfer gap of Cr_2O_3 at 3.3 eV, the absorption length of the pump pulses was ~ 7 μm.[21]

SHG by pulses emitted from an optical parametric amplifier pumped by the Ti:sapphire laser was employed for probing the dynamical properties. As shown in Fig. 1(a), the samples were mounted in a cryostat and SHG from the region excited by the pump beam was measured in transmission. In order to ensure that a uniformly pumped area is probed, the diameter of the probe beam is 50% smaller than that of the pump beam. Furthermore, the SHG energy $2\hbar\omega_{probe}$ was chosen such that the absorption length at $2\hbar\omega_{probe}$ (here 1.7 μm at 2.0 eV) was much smaller than the absorption length at $\hbar\omega_{pump}$. Furthermore, because of the large absorption, the issue of phase matching can be neglected.[14]

The intensity of the probe beam was in the order of 10 mJ/cm^2, but this can still be regarded as "weak" in comparison to the pump beam because of the negligible absorption of the probe beam in the sample. In both setups, wave plates and foil polarizers were applied to set the polarization of the incoming light and to analyze the polarization of the SHG light, respectively. Color filters were used in front of the sample for suppressing SHG generated in optical components and behind the sample for separating the SHG light from the fundamental light. The SHG signal was detected by a GaAs photomultiplier tube and normalized to the squared intensity of the transmitted fundamental light.

It is known that the phase of the SHG light can carry important information about the magnetic state which is absent in the amplitude.[11] We therefore require a setup in which both the amplitude A of and the phase φ between spin and lattice contributions to the SHG signal are measured with high accuracy. This was achieved by mounting the components, which set and analyze the polarization of the light waves, in computer controlled mechanical rotors. This allowed us to measure the polarization configurations needed for the determination of the SHG amplitudes and phases [see Fig. 1(b)] in one experimental run. Avoiding the temporal drift of consecutively measured data sets, we were able to determine the temporal evolution of φ with an accuracy of 0.1°.

V. EXPERIMENT

A. Second-harmonic-generation spectra

Figures 1(c) and 1(d) show the spectral dependence of SHG from Cr_2O_3 at 10 K in the range 1.7–3.0 eV. As described, the four spectra were measured in a single experimental run in contrast to previous experiments. The configurations displayed in Fig. 1(b) were applied in order to obtain them. The settings of polarizer and analyzer are based on Eqs. (2) and (3). The magnetic and crystallographic contributions to SHG are generated with y-polarized fundamental light and separated by detecting the y- and x-polarized component of the SHG light, respectively. The SHG intensities are $I_{\mathrm{mag}} \propto |S_y|^2$ and $I_{\mathrm{cryst}} \propto |S_x|^2$, with $\vec{S}(2\omega)$ as source term from Eq. (1). The constructive and destructive interferences of magnetic and crystallographic SHG contributions are obtained with circularly polarized incident light and no analyzer in the SHG beam. Here, the SHG intensities are $I_{\pm} \propto |S_y \pm iS_x|^2$. The amplitude of the magnetic contribution, which is proportional to the AFM order parameter, and the amplitude of the crystallographic contribution (for convenience denoted by L) are

$$A_{\mathrm{mag}} = \sqrt{I_{\mathrm{mag}}} \propto \ell, \quad A_{\mathrm{cryst}} = \sqrt{I_{\mathrm{cryst}}} \equiv L. \tag{4}$$

The relative phase φ between the magnetic and crystallographic contributions[22] is given by

$$\sin\varphi = \frac{I_+ - I_-}{I_+ + I_-} \cdot \frac{I_{\mathrm{mag}} + I_{\mathrm{cryst}}}{2\sqrt{I_{\mathrm{mag}} I_{\mathrm{cryst}}}}. \tag{5}$$

In Refs. 23 and 24, it was shown that the origin of magnetic SHG in Cr_2O_3 is a twisted octahedral ligand field in combination with spin-orbit interaction which leads to two-photon electric-dipole transitions coupling to the AFM order parameter. The value of φ is determined by local-field corrections to the magnetic and crystallographic SHG susceptibilities. This relation is a complex one and prevents the derivation of quantitative values for ℓ and L from φ. However, as we will see in the following, the phase of the SHG signal can still be employed as qualitative probe of the magnetization and the lattice dynamics, which reveals important information about the temporal evolution of the spin-lattice interaction that is not acquired from the intensity of the SHG signal.

According to Eq. (5), in order to minimize the error of $\Delta\varphi$, the phase should be measured at a photon energy where $I_+ \gg I_-$ and $I_{\mathrm{mag}} \approx I_{\mathrm{cryst}}$. Figure 1 reveals that SHG in the range 1.9–2.2 eV or near 2.6 eV meets these requirements. The optical parametric amplifier can emit light at 0.55–0.77 eV ("idler") and at 0.77–1.00 eV ("signal"). For probing at SHG energies >2.0 eV, i.e., fundamental energy >1.0 eV, the frequency doubled idler wave needs to be used as probe wave. However, the intensity of this wave is too low, so that in spite of the larger SHG efficiency near 2.2 eV, the fundamental signal wave was used for probing the ultrafast SHG response at 2.0 eV.

B. Pump-and-probe data

Figure 2(a) shows the temporal evolution of the change of SHG intensity ΔI after exciting a Cr_2O_3 sample at 285 K with a 250 fs pump pulse with an intensity of 10 mJ/cm^2. The zero position of the delay t is defined by the maximum of the cross correlation in Fig. 2(c). Two regimes with a basically different SHG response are observed. At $t < 0.3$ ps, the response is universal: A transient decrease of all SHG signals by about 10% occurs. At $t > 0.3$ ps, the temporal evolution of SHG is drastically different for the four configurations with ΔI ranging from −22% to +18%.

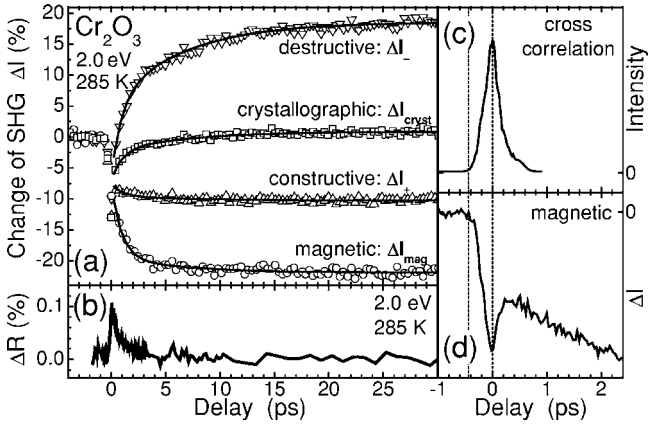

FIG. 2. Temporal evolution of SHG signals in a pump-and-probe experiment. (a) Change of SHG intensity ΔI at 2.0 eV versus delay t after the photoexcitation. Based on Fig. 3(b), an instantaneous and two exponential contributions are fitted to the data (see text) and lead to the solid lines. Note that each curve is fitted with the same time constants (τ_2=0.93 and τ_3=6.62 ps). (b) Change of linear reflectivity ΔR at 2.0 eV versus delay t after the photoexcitation. (c) Cross correlation of pump and probe pulses. (d) Superposition of magnetic contribution to SHG and optical effects modifying the SHG intensity near t=0.

In the interpretation of these data, optical effects modifying merely the efficiency of the SHG process must be distinguished from SHG variations that are due to a genuine change of magnetization or lattice temperature.[25] On the one hand, the efficiency of the SHG process is modified by changes of the linear optical constants that change the intensity of the fundamental light entering the sample and of the SHG light leaving the sample. Figure 2(b) shows that the pump beam leads to a change of reflectivity ΔR at the SHG wavelength by $\leqslant$0.1% (the same result is obtained at the fundamental wavelength). Modification of the linear optical properties can therefore be neglected in Fig. 2(a). On the other hand, the efficiency of the SHG process is modified by nonlinear interaction between the pump and probe waves and by the massive excitation of nonequilibrium carriers in the presence of the pump beam. In agreement with other pump-and-probe experiments based on SHG,[12,13,26] the universal dip at t=0 in Fig. 2(a) is ascribed to these effects. The kink at t=0.3 ps in Fig. 2(d) indicates the transition from the range dominated by optical effects to the range displaying genuine spin and lattice dynamics.

Figures 3(a) and 3(b) show the temporal evolution of the following parameters: (i) the change of the AFM order parameter $\Delta\ell$, (ii) the change of the corresponding lattice contribution ΔL, and (iii) the change of the relative phase be-

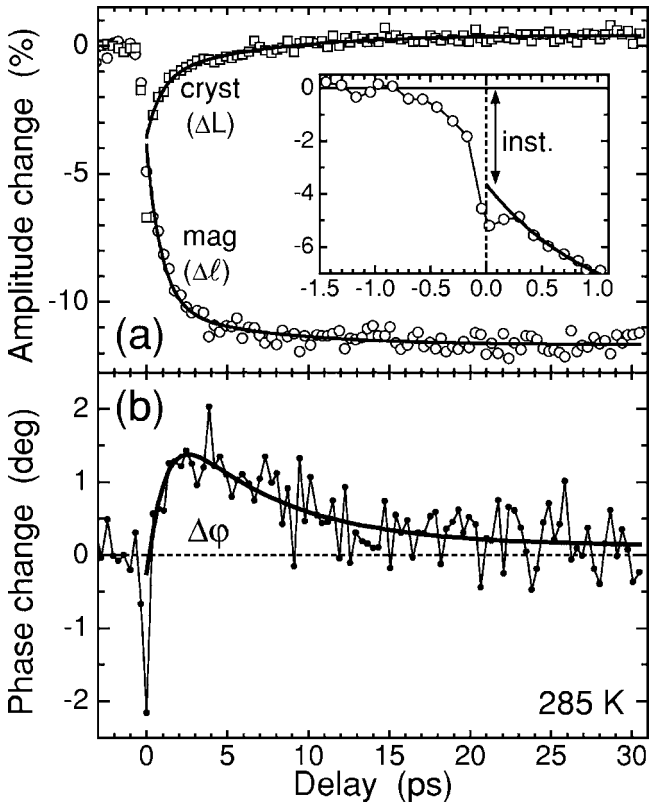

FIG. 3. Temporal evolution of the change of (a) amplitude and (b) phase. Data and solid lines are derived from Fig. 2(a) using Eqs. (4) and (5). The inset shows the extrapolation to $t=0$ in comparison to the SHG data. This reveals the instantaneous demagnetization (arrow) discussed in the text.

tween spin and lattice contributions to SHG $\Delta\varphi$ as derived from the raw data in Fig. 2(a) by means of Eq. (5). The progression in Fig. 3(a) does not uniquely reveal the number of channels contributing to $\Delta\ell(t)$ and $\Delta L(t)$. However, this is disclosed by the temporal evolution of $\Delta\varphi$ in Fig. 3(b). A repeated change of the sign of the slope of $\Delta\varphi(t)$ shows that three independent channels with alternating sign of the associated phase change contribute. Based on this observation, three processes are fitted to the data at $t>0.3$ ps in Fig. 2(a). The processes are (i) an "instantaneous" contribution on a time scale $\tau_1 \ll 1$ ps described by a step, (ii) a "fast" exponential contribution with a characteristic time $\tau_2=0.93$ ps, and (iii) a "slow" exponential contribution with a characteristic time $\tau_3=6.62$ ps. The excellent agreement between data and fits in Fig. 2 and, consequently, in Fig. 3 confirms the presence of three channels. It further demonstrates that even without establishing a quantitative relation between $\Delta\varphi$ and $(\Delta\ell, \Delta L)$, the phase serves as valuable probe of the magnetization and lattice dynamics.

C. Model

Figure 3 leads us to the following scenario. Following previous experiments, the instantaneous process is ascribed to emission of magnetic excitations such as magnons during nonradiative decay of photoexcited carriers.[3] Subsequently, ΔL reproduces the lattice temperature. This is confirmed by the correspondence of $\Delta L(t)$ and $-\Delta R(t)$. The reflectivity change reproduces the temperature of the photogenerated carriers[27] and, thus, of the lattice because thermal equilibrium of electrons and lattice is acquired within <1 ps.[28] Furthermore, $\Delta\ell$ reproduces the spin temperature, which is governed by spin-lattice interaction via the fast and the slow processes. Spin-lattice interaction is evidenced by the fact that the lattice temperature is decreasing (increase of ΔL) while the spin temperature is increasing (decrease of $\Delta\ell$), with $\Delta L(t)$ and $\Delta\ell(t)$ being described by the *same* relaxation times τ_1 to τ_3. With 307.6 K as the Néel temperature, $\Delta\ell(30\ \text{ps})=-12\%$ corresponds to a spin temperature increase by 9 K at 285 K, which coincides with the value calculated for lattice heating by the pump pulse.[21,29] On the other hand, the SHG intensity of the lattice contribution is mostly determined by the gradual increase of linear absorption with temperature,[21] which attenuates the SHG wave by about 1%-10% per 100 K. Here, a temperature increase by 9 K is a very small effect and explains the near recovery of $\Delta L(30\ \text{ps})$. Note that electron-spin interaction is negligible because Cr_2O_3 is an insulator. Thermal diffusion is also negligible because it occurs on a time scale of >300 ps.[28]

The data in Fig. 3 reveal two remarkable differences to the dynamical processes of ferromagnetic (and ferrimagnetic) compounds: First, *two* demagnetization channels, the slow and the fast process, mediate the thermalization of spins and lattice, whereas in ferromagnets only one such channel was observed.[3,30] The difference is striking but its origin is yet unclear. Second, the demagnetization times $\tau_{2,3}$ are 2 orders of magnitude *shorter* than the demagnetization time for a ferromagnetic compound[3] with the same magnetocrystalline anisotropy constant ($K_A=8\times10^4$ erg/cm^3 at room temperature[31]) as Cr_2O_3. This is understood as follows. In Ref. 3, it is shown that the demagnetization time for a ferromagnetic compound scales inversely with the ferromagnetic resonance frequency, which is proportional to the magnetic anisotropy energy: $\omega_{\text{FM}} \propto E_A$. In analogy, it is reasonable to assume that the demagnetization time for an AFM compound scales inversely with the AFM resonance frequency. The AFM resonance frequency is given by

$$\omega_{\text{AFM}} \propto \sqrt{E_A E_{ex}}, \tag{6}$$

with E_{ex} as exchange energy.[32] For Cr_2O_3, one finds a ratio[31] $E_{ex}/E_A \sim 10^4$, which leads to the 2 orders of magnitude faster response observed.

Note that the excellent agreement of fits and data in Fig. 3 allows one to extend the progression of $\Delta\ell(t)$ to $t=0$ and to separate the AFM contributions to SHG from optical modifications of the SHG efficiency in that range. The result in the inset of Fig. 3 reveals the instantaneous contribution.

D. Temperature dependence

Figure 4(a) shows the temporal evolution of the change of the AFM order parameter at three temperatures. The transient drop of SHG intensity due to modification of the SHG efficiency by the pump pulse up to $t\sim0.3$ ps appears at all temperatures. At 250 K, the instantaneous and the slow process

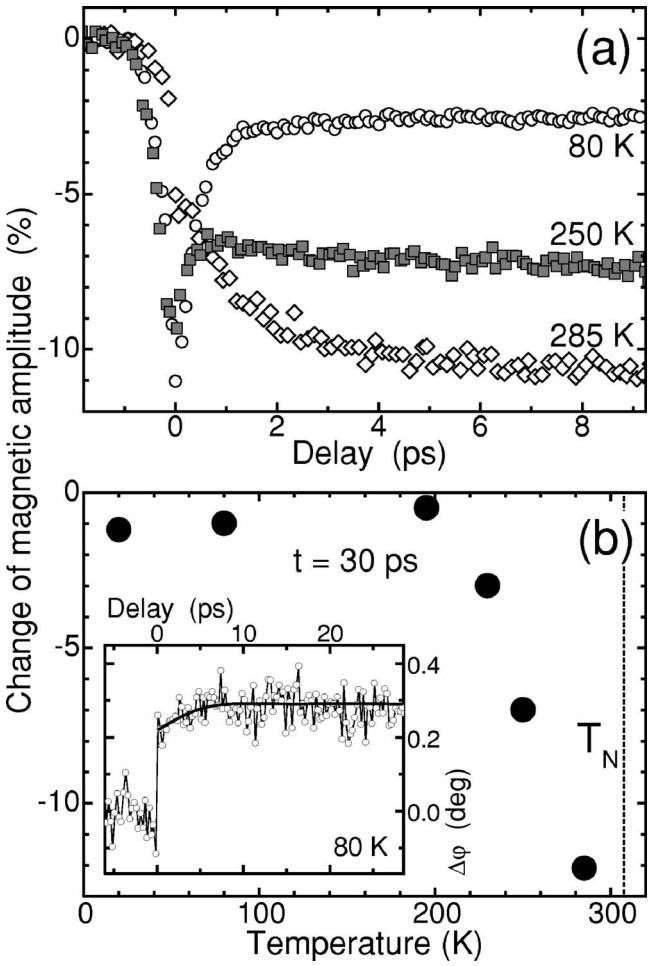

FIG. 4. Temperature dependence of the magnetization dynamics. (a) Evolution of the change of amplitude of magnetic SHG at three temperatures. (b) Change of magnetic amplitude at $t=30$ ps as a function of temperature. Inset: evolution of the change of phase $\Delta\varphi$ at 80 K.

are also observed but less pronounced than at 285 K. For the slow process, the fit reveals $\tau_3=6.23$ ps. Because of the smaller magnitude, the fast process can no longer be separated from the optical effects modifying the SHG intensity at $t<0.3$ ps. At 80 K, the magnitude of both the fast and the slow process is too small to be resolved, and only the instantaneous change of magnetization is observed. Again, the temporal evolution of the phase change reveals additional information: The inset of Fig. 4 shows that the slow process still plays a role at 80 K, since a reproducible increase of $\Delta\varphi$ on a time scale $\tau_3=5.2$ ps is observed.

First, Fig. 4(b) confirms that an instantaneous demagnetization is present at all temperatures below T_N, whereas slower demagnetization processes become relevant near T_N only.[3] Second, the fits reveals a continuous decrease of τ_3 with temperature. According to Eq. (6), this is consistent with the increase of the magnetic anisotropy with decreasing temperature because of $\tau_3 \propto \omega_{\mathrm{AFM}}^{-1}$. The correspondence is a qualitative, not a quantitative, one because the temperature dependence of the magnetic specific heat[30] can also influence the temperature dependence of τ_3.

VI. CONCLUSION

In summary, the dynamical processes in AFM bulk Cr_2O_3 after excitation with an intense laser pulse were investigated by ultrafast optical pump-and-probe experiments. SHG coupling either to the magnetic or the crystallographic subsystems allows us to separate the spin dynamics from the lattice dynamics and to study the interaction of these subsystems. Phase resolved SHG reveals that three thermalization processes contribute to the demagnetization on time scales of $\ll 1$, 0.93, and 6.62 ps at $T=285$ K. The first process is associated with emission of magnetic excitations during nonradiative carrier decay, whereas the latter two describe the thermalization of the spin system by spin-lattice interaction. Our results demonstrate that the magnetization dynamics of even a simple AFM model compound differs noticeably from that of ferromagnetic compounds.

In future experiments, the potential of nonlinear optical techniques to distinguish between contributions from different sublattices of a sample just on the basis of polarization selection rules and spectroscopy will be used to investigate the dynamical relations between sublattices in multiply ordered compounds. Here, multiferroics with a coexistence of (anti)ferroelectricity and (anti)ferromagnetism are candidates of great current interest.

ACKNOWLEDGMENTS

The authors thank M. Matsubara for help with the reflection measurements. Subsidy from the SPP 1133 of the DFG is appreciated. M.F. thanks T. Elsässer for continuous support.

*Present address: Department of Basic Science, The University of Tokyo, Komaba, Meguro-ku, Tokyo 153-8902, Japan.
†Present address: ECN, Afdeling zonne-energie, P.O. Box 1, 1755 ZG Petten, The Netherlands.
‡Present address: ITIMS, Hanoi University of Technology, 1 Dai Co Viet Road, Hanoi, Vietnam.
§Present address: SSP-ERATO, Japan Science and Technology Agency, Tsukuba, Ibaraki 305–8562, Japan.
‖Present address: HISKP, Universität Bonn, Nussallee 14–16, 53115 Bonn, Germany. Electronic address: fiebig@hiskp.uni-bonn.de

[1] A. V. Kimel, A. Kirilyuk, F. Hansteen, R. V. Pisarev, and T. Rasing, J. Phys. Condens. Matter **19**, 043201 (2007).
[2] *Spin Dynamics in Confined Magnetic Structures*, edited by B. Hillebrands and K. Ounadjela (Springer, Heidelberg, 2006).
[3] T. Ogasawara, K. Ohgushi, Y. Tomioka, K. S. Takahashi, H. Okamoto, M. Kawasaki, and Y. Tokura, Phys. Rev. Lett. **94**, 087202 (2005).
[4] *Colossal Magnetoresistive Oxides*, edited by Y. Tokura (Gordon

and Breach, London, 2000).
[5] S. S. P. Parkin *et al.*, J. Appl. Phys. **85**, 5828 (1999).
[6] A. V. Kimel, R. V. Pisarev, J. Hohlfeld, and Th. Rasing, Phys. Rev. Lett. **89**, 287401 (2002).
[7] A. V. Kimel, A. Kirilyuk, A. Tsvetkov, R. V. Pisarev, and Th. Rasing, Nature (London) **429**, 850 (2004).
[8] M. Fiebig, K. Miyano, Y. Tomioka, and Y. Tokura, Appl. Phys. B: Lasers Opt. **71**, 211 (2000).
[9] G. Ju, A. V. Nurmikko, R. F. C. Farrow, R. F. Marks, M. J. Carey, and B. A. Gurney, Phys. Rev. Lett. **82**, 3705 (1999).
[10] M. Fiebig, V. V. Pavlov, and R. V. Pisarev, J. Opt. Soc. Am. B **22**, 96 (2005).
[11] A. Kirilyuk, J. Phys. D **35**, R189 (2002).
[12] J. Hohlfeld, E. Matthias, R. Knorren, and K. H. Bennemann, Phys. Rev. Lett. **78**, 4861 (1997).
[13] N. P. Duong, T. Satoh, and M. Fiebig, Phys. Rev. Lett. **93**, 117402 (2004).
[14] Y. R. Shen, *The Principles of Nonlinear Optics* (Wiley, New York, 1984).
[15] This is not to be confused with the electric and magnetic multipole expansions of the source term $\vec{S}$, which does not refer to the ordered crystal but to the electric- and magnetic-field components of the light fields involved (Ref. 10). In Cr_2O_3, the "crystallographic" SHG contribution $\propto\hat{\chi}(0)$ is of the magnetic-dipole type whereas the "magnetic" SHG contribution $\propto\hat{\chi}(\ell)$ is of the electric-dipole type (Ref. 20).
[16] P. Borisov, A. Hochstrat, X. Chen, W. Kleemann, and C. Binek, Phys. Rev. Lett. **94**, 117203 (2005).
[17] M. Fiebig, J. Phys. D **38**, R123 (2005).
[18] *Numerical Data and Functional Relationchips*, edited by K. H. Hellwege and O. Madelung, Landolt Börnstein, New Series, Group III, Vol. 17, Pt. G (Springer, Berlin, 1984).
[19] J. S. Dodge, A. B. Schumacher, J. Y. Bigot, D. S. Chemla, N. Ingle, and M. R. Beasley, Phys. Rev. Lett. **83**, 4650 (1999).
[20] M. Fiebig, D. Fröhlich, B. B. Krichevtsov, and R. V. Pisarev, Phys. Rev. Lett. **73**, 2127 (1994).
[21] D. S. McClure, J. Chem. Phys. **38**, 2289 (1963).
[22] The *absolute* phase of the spin contribution (φ_{spin}) or lattice contribution (φ_{lattice}) to SHG can be determined by interfering the respective contribution with SHG light from a reference source (e.g., a quartz crystal). However, for the present experiment, it is sufficient to determine the *relative* phase ($\varphi=\varphi_{\text{spin}}-\varphi_{\text{lattice}}$) by interfering spin and lattice contributions to SHG.
[23] M. Muto, Y. Tanabe, T. Iizuka-Sakano, and E. Hanamura, Phys. Rev. B **57**, 9586 (1998).
[24] Y. Tanabe, M. Muto, M. Fiebig, and E. Hanamura, Phys. Rev. B **58**, 8654 (1998).
[25] B. Koopmans, M. van Kampen, J. T. Kohlhepp, and W. J. M. de Jonge, Phys. Rev. Lett. **85**, 844 (2000).
[26] C. Guo, G. Rodriguez, and A. J. Taylor, Phys. Rev. Lett. **86**, 1638 (2001).
[27] C. K. Sun, F. Vallee, L. H. Acioli, E. P. Ippen, and J. G. Fujimoto, Phys. Rev. B **50**, 15337 (1994).
[28] S. K. Sundaram and E. Mazur, Nat. Mater. **1**, 217 (2005).
[29] C. T. Anderson, J. Am. Chem. Soc. **59**, 488 (1937).
[30] R. D. Averitt, A. I. Lobad, C. Kwon, S. A. Trugman, V. K. Thorsmølle, and A. J. Taylor, Phys. Rev. Lett. **87**, 017401 (2001).
[31] S. Foner, Phys. Rev. **130**, 183 (1963).
[32] C. Kittel, Phys. Rev. **82**, 565 (1951).